



Optimisation of Trapped Vortex Cavity for Airfoil Separation Control

C. Panigrahi, R. Chawla and M. T. Nair[†]

*Department of Aerospace Engineering, Indian Institute of Space Science and Technology,
Thiruvananthapuram, Kerala, 695547, India*

[†] *Corresponding Author Email: manojtnair.iist@gmail.com*

(Received February 8, 2021; accepted August 7, 2021)

ABSTRACT

The effects of a Trapped Vortex Cavity (TVC) on the aerodynamic performance of a NACA 0024 airfoil at a constant angle of attack (AoA) of 14° were investigated in this study. It was observed that mass suction (MFR) was required to stabilise the vortex within the cavity segment. Lift to drag ratio (L/D) and MFR were chosen as performance objectives, along with a fully attached flow constraint (flow separation at $X/c \geq 95\%$). Parametric analysis was carried on the baseline airfoil with and without suction and compared to the airfoil with TVC with and without suction. It was observed that L/D increases as MFR increases for a baseline airfoil, and flow separation is delayed at high suction values (MFR = 0.2 kg/s). The TVC modifies the pressure distribution on the baseline airfoil when MFR is applied to the cavity section and there is a significant increase in lift; thus, L/D increases and flow separation is delayed. A lower value of MFR = 0.08 kg/s is sufficient to stabilise the vortex and improve the efficiency of the TVC airfoil. The findings of these parametric studies were used to do a multi-objective optimisation using a genetic algorithm to attain the desired cavity shape while achieving the largest L/D and the lowest MFR (that is proportional to the power required for control) with a fully attached flow constraint. It was found that mass suction and cavity shape both had an equal influence on flow control. The Pareto optimal front yielded a series of optimum designs. One of them was subjected to an off-design analysis in order to validate its performance at other incidences. It was observed that it performs better than the baseline airfoil, with an improved L/D and an increase in stall angle from 10° to 14°.

Keywords: Airfoil; Vortex; Cavity; Flow separation; Multi-objective optimisation; Genetic algorithm; Mass suction; Turbulence.

NOMENCLATURE

AoA	angle of attack	MFR	Mass Flow Rate
c	chord length	MOGA	Multi-Objective Genetic Algorithm
c_l	coefficient of lift	RANS	Reynold's Averaged Navier Stokes Equation
c_d	coefficient of drag	TVC	Trapped Vortex Cavity
c_p	coefficient of pressure	TVCS	Trapped Vortex Cavity With Suction
c_f	coefficient of skin friction	ULH	Uniform Latin Hypercube
L / D	lift to drag ratio		

1. INTRODUCTION

With the current boom in the aircraft industry, manufacturers worldwide aim to carry larger loads efficiently. New generation aircraft have efficient wings with a high lift to drag ratio to reduce fuel consumption and make business more profitable. Various techniques have been used to increase the

efficiency of wings, such as slats and flaps. However, this increases the structural mass of the wing. Thicker wings are needed to build larger aircraft, resulting in reduced efficiency and flow separation at low angles of attack. At higher angles of attack, if the separation point on the airfoil can be pushed back, it can result in a cleaner flow on the upper surface of the airfoil and thus, increase its efficiency. The

fundamental purpose of this research is to improve the efficiency of an airfoil through the use of a flow control approach. Flow control techniques can be categorized in two ways, i.e. passive control requiring no auxiliary power and active control requiring open loop or closed loop power supply. One of the flow control strategies is referred to as the Trapped Vortex cavity (TVC). Here, an airfoil with a cavity positioned on the upper surface is designed. A vortex is anchored inside it, creating a large recirculation region to delay the separation of flow. The idea of capturing a vortex to attach a flow to an airfoil is quite old, as referred to in Ringleb (1961). Kasper (1975) claimed the first successful use of the trapped vortex in a flight experiment. Adkins (1975) demonstrated the usage of stabilised trapped vortex in a short diffuser to achieve pressure recovery. Iollo and Zannetti (2001) have shown that a trapped vortex can have a limited stability region. The vortex is unstable under certain conditions and cannot be kept trapped if some control in the cavity region is not exerted. Rowley *et al.* (2005) showed that the global effect of the cavity on the flow around the airfoil is the generation of vortices that reduce flow separation downstream of the cavity. PIV measurements on a cavity located on an airfoil have been carried out by De Gregorio F (2008) suggesting that a coherent vortex can be formed if suction was applied in the cavity region. The studies are limited to an airfoil cross-section, and not many experiments have been conducted to provide the effectiveness of the TVC flow control technique over a wing profile. Most of the work on cavity flows have focused on simpler geometries such as rectangular cavities, which is practically unsuitable for trapping a vortex on the wing. However, the fundamental flow mechanisms observed in such a configuration provide insight for using it in a flow control application. Cavity flows are characterised by self-sustained oscillations, which are a function of incoming flow parameters and cavity geometries as suggested by Rossiter (1964), Rockwell and Naudascher (1979) and Rowley *et al.* (2001). Olsman and Colonius (2011) studied the complex flow physics arising from the interaction of cavity flow with the external flow and suggested that the oscillations generated in the vortices delayed separation. Lasagna *et al.* (2011) also reported promising results for a wing cross section with a vortex cavity and blowing air by injecting flow into the cavity. The pressure fluctuations observed in the cavity suggested a very complex interaction of flow features and drag modes that could be characterised similar to those of the unsteady phenomenon observed in the rectangular cavity flows.

VORTEX CELL 2050 was an European research project established to examine the various levels of complexity related to the concept of TVC in an airfoil and demonstrate the right design of cavity shapes to trap flow vortices; hence, minimize pressure drag past bluff bodies/thick wing airfoils. The research group conducted various wind tunnel experiments as shown in Donelli *et al.* (2009) and many CFD studies as observed in Donelli *et al.* (2010) to conclude that practically anchoring a vortex inside the cavity is difficult without an active

mechanism. An active mass suction and a good cavity shape are necessary to stabilise the vortex inside the cavity, as illustrated in Donelli *et al.* (2010) and Donelli *et al.* (2011). Vuddagiri and Samad (2013) performed unsteady simulations of flow over an airfoil with and without cavities and found that the airfoil with a cavity produced greater drag and less lift than the airfoil without a cavity.

Many of these studies focused on obtaining the suction (MFR) needed to trap a vortex in a given cavity shape, and the distribution of MFR in the cavity was not studied. This motivated the current study, in which, the form of the cavity and the distribution of the MFR are adjusted simultaneously to delay separation on the airfoil's upper surface and therefore, obtain a greater L/D. In the VORTEX CELL 2050 studies, it was discovered that it is impossible to stabilise the vortex inside the cavity without a suction system at high angles of incidence, such as AoA=14° or higher (Donelli *et al.* 2009). Thus, this AoA was taken up for the study.

Thick airfoils are structurally advantageous for a wing design; however, increasing the thickness decreases airfoil efficiency. They are prone to flow separation at low angles of attack. Hence, to prove the efficiency of the concept of trapped vortex cavity, in this paper, a NACA 0024 airfoil is taken as the baseline airfoil, and the cavity shape is designed using a third-order Bezier curve whose location has been fixed on the upper surface. Parametric studies have been carried out for the baseline airfoil with and without suction (MFR) and Trapped Vortex Cavity (TVC) airfoil with and without MFR. A parametric study for the distribution of MFR is also carried out. Based on the results obtained from the parametric studies, a multi-objective optimisation study was done using a genetic algorithm to obtain the desired cavity shape to achieve the maximum L/D and at minimum MFR with a constraint of fully attached flow. Then, the most optimised design obtained from the Pareto optimal front was taken. An off-design analysis was carried out to verify its performance at other incidences, and results were compared with that of the baseline airfoil.

2. PROBLEM STATEMENT

A baseline NACA 0024 airfoil with a chord length of 1m is taken. The study was done at an AoA of 14° with the input parameters given in Table 1.

Table 1. Initial conditions used in the study

Parameters	Values
Fluid	Air
Freestream Pressure	101325 Pa
Freestream temperature	298 K
Freestream velocity	30 m/s
Re	2×10^6
Scheme	Point-implicit
Turbulence model	$k-\omega$ SST

The cavity shape and mass flow rate are optimised to trap the vortex inside the cavity with a delayed flow separation constraint. The multi-objective problem statement for optimisation is given below.

Objective:

$$M = w_1 \times \frac{L}{D} - w_2 \times \text{MFR}$$

Maximize : M | @ Flow separation instant

w.r.t:

$$(X_i, Y_i) \text{ where } i = 1, 2 \dots 4$$

where X and Y - coordinates describe the shape of the airfoil.

Constraints:

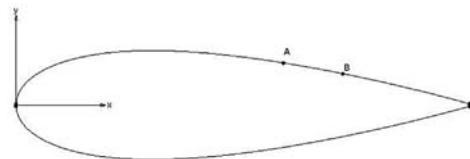
$$\frac{X_{\text{flow separation}}}{c} \geq 95\%$$

$$Y_1 < 40\% \times \frac{t_{\text{max}}}{c}$$

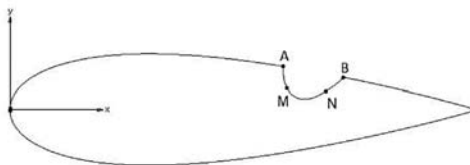
$$\frac{X}{c} = 0.58 \leq W_{\text{cavity}} \leq \frac{X}{c} = 0.69$$

Where, $X_{\text{flow separation}}$ is the point of flow separation on the upper surface of the airfoil, W_{cavity} is the width of the cavity segment on the airfoil i.e. Point A to Point B in Fig. 1 and t_{max} is the maximum camber on the airfoil.

In Fig. 1b, a typical Trapped Vortex Cavity (TVC) airfoil shape is shown with segment M to N as the segment in which suction is applied.



(a) Baseline airfoil NACA 0024



(b) NACA 0024 TVC airfoil

Fig. 1. Airfoils used in the study.

3. CAVITY DESIGN AND PARAMETERISATION

Two third-order Bezier curves are used to create the shape of the cavity as it gives enough freedom to get an optimised shape. The maximum allowable depth of the cavity is fixed at $40\% \times \frac{t_{\text{max}}}{c}$ taking into

account the structural strength of the wing. The starting and ending point (Point A and B in Fig. 1b) of the cavity on the airfoil is also fixed. To design a 2D cavity of two 3rd order Bezier curves, 8 parameters are required as shown by Piegel and Tiller (1996).

4. GRID INDEPENDENCE STUDY

Grids around the NACA 0024 airfoil with and without a cavity were generated using Pointwise grid generating software. A hybrid grid was used, consisting of quadrilateral cells on the exterior of the airfoil and triangular cells within the cavity. Around the airfoil and the cavity periphery, a structured grid (45 layers of quadrilateral elements) was created in the boundary layer region normal to the wall direction. The first grid cell centre is positioned at a distance of $\Delta S = 1.2 \times 10^{-5}$ from the wall in order to perform wall resolved turbulence modelling. This initial cell placement corresponds to $y^+ = 1$ and is used for all computational grids (Table 3) utilised in this investigation to effectively capture the viscous boundary layer. The airfoil was discretised along its length, excluding the cavity, using 270 elements stretched near the trailing edge and cavity starting and endpoints. The cavity periphery was discretised using 180 elements, and a structured grid (40 layers of quadrilateral elements) was generated in the shear layer across the cavity opening. The rest of the cavity domain was filled with an unstructured grid. The grid employed in the computational investigation is given in Fig. 2.

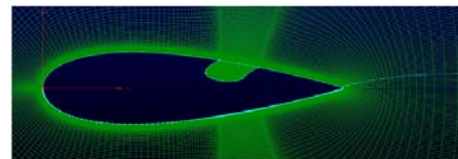


Fig. 2. Computational grid.

A grid independence study was carried out and tabulated as shown in Table 2 and Fig. 3. Grid-3 was selected based on the results as it can be observed that there was no significant change in c_l and c_d with a change in grid size for grids 3-5. The X-axis represents the grids, while the other two axes are c_l and c_d . The details of Grid-3 are given in Table 3.

Table 2. Results of grid independence study

Grid	No. of cells	c_l	c_d
Grid-1	52848	1.16	0.0307
Grid-2	54683	1.15	0.0303
Grid-3	84692	1.14	0.0309
Grid-4	107596	1.14	0.0311
Grid-5	108694	1.14	0.0313

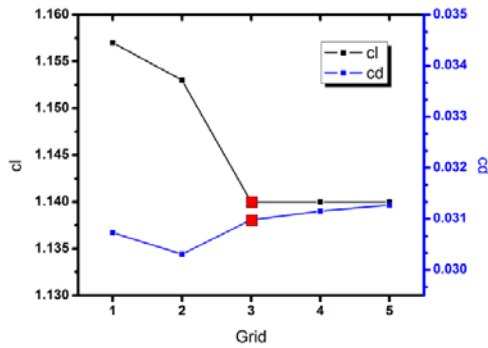


Fig. 3. Results of grid independence study.

Table 3. Details of the computational grid used

Total no. of cells	84692
ΔS	1.2×10^{-5}
Re	2×10^6
y^+	1

The grid generation process was automated, where the baseline NACA 0024 airfoil was used as the base geometry. A script was written to take into account the geometrical parameters of the Bezier curve to determine the shape of the cavity. The same was executed in the form of a new design. The process takes the coordinates as input from the design of the experiment table, changes their values in the script file, generates a new geometry of the cavity shape on the baseline NACA 0024 geometry, and saves these files along with the necessary boundary condition and input files for the CFD++ solver.

5. CFD SETUP

Metacomp CFD++ has been used to perform numerical simulations. The solver uses the Reynolds Averaged Navier-Stokes (RANS) flow equation on hybrid grids using the finite-volume method. The preconditioned density-based scheme has been applied. The $k-\omega$ SST turbulence model has been used since it can accurately reproduce flows inside the trapped cavities as shown by Ringleb (1961) and Olsman and Colonius (2011).

5.1 Initial conditions

All the cases were run at a constant AoA of 14° with the initial conditions as shown in Table 1.

5.2 Boundary conditions

The turbulent viscosity ratio $\left(\frac{\mu_t}{\mu}\right) = 1.5$ and turbulence intensity $I_t = 0.1$ were set in accordance with the inlet free stream conditions of 30 m/sec as in Kasper (1975). Classic adiabatic wall with no slip condition was given on the airfoil walls and inside the cavity. In segment M to N of Fig. 1b wall bleed (suction) condition was applied for different value of

MFR's. Figure 4 shows the typical boundary condition used in the study.

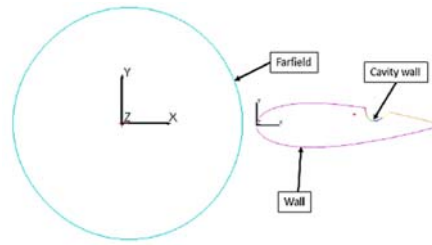


Fig. 4. Boundary conditions used in the study.

5.3 CFD validation

CFD validation was carried out for the NACA 0024 baseline airfoil and compared with the results obtained using XFLR5 code with the initial conditions as shown in Table 1. It was observed that the aerodynamic coefficients c_l and c_d obtained from the CFD study are in close agreement with those obtained from XFLR5 code as shown in Fig. 5 and Fig. 6 respectively. Also shown are the experimental results from Lasagna *et al.* (2011) at $Re = 1 \times 10^6$. The comparison with Lasagna *et al.* (2011) is good for c_d , however, c_l is seen to be higher at higher angles of attack in the present case.

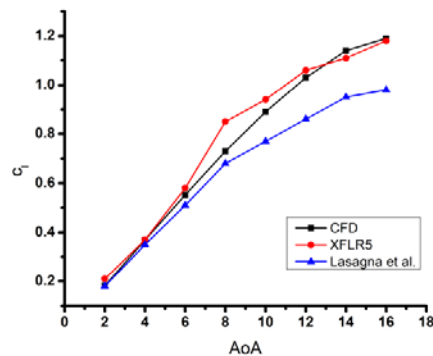


Fig. 5. c_l vs AoA for baseline airfoil.

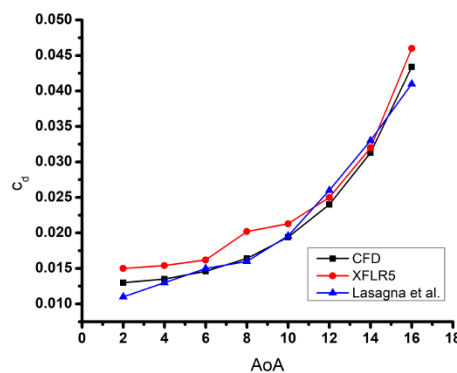


Fig. 6. c_d vs AoA for baseline airfoil.

6. PARAMETRIC ANALYSIS

6.1 Parametric study on baseline NACA 0024 airfoil with different MFRs

A parametric study was conducted on the baseline NACA 0024 airfoil without a cavity to determine the effects of uniformly distributed MFR suction applied in the segment A to B of Fig. 1a. The obtained results are summarised in Table 4.

Separation point and the value of c_l increase as the MFR value increases as it directly affects the state of the boundary layer on the body. The variation of c_l with MFR is seen in Fig. 7. An increase in MFR should also decrease c_d as the flow separation is delayed. However, a different trend is observed. Apart from the value of MFR, its distribution in segments A to B, as shown in Fig. 1a, also plays a vital role. The c_d decreases for the initial values of MFR. However, at AoA of 14° as the MFR value increases, one of its components (in +X direction as shown in Fig. 1) also acts in the drag direction,

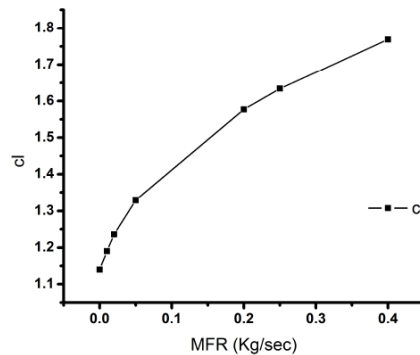


Fig. 7. c_l vs MFR for baseline NACA 0024 airfoil.

increasing c_d as shown in Fig. 8. The L/D increases initially with an increase in MFR but decrease with a further increase in MFR, as shown in Fig. 9.

The pressure contour of the baseline airfoil NACA 0024 along with the velocity streamlines without any mass suction is shown in Fig. 11. Without mass suction, the flow on the airfoil's upper surface separates at roughly 70% of X/c , resulting in the formation of a recirculation area.

Table 4. Baseline NACA0024 airfoil with various MFR's

MFR (kg/sec)	c_l	c_d	L/D	Point of Separation (% X/c)
0.00	1.14	0.031	36.4	70.4
0.01	1.19	0.029	41.7	75.2
0.02	1.24	0.027	46.0	78.7
0.05	1.33	0.024	54.6	85.6
0.20	1.58	0.024	65.2	95.8
0.25	1.63	0.025	64.5	97.1
0.40	1.77	0.030	58.8	99.3

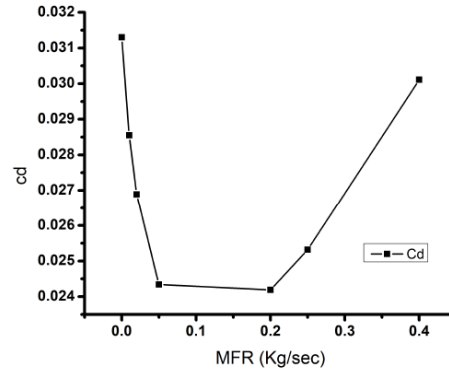


Fig. 8. c_d vs MFR for baseline NACA 0024 airfoil.

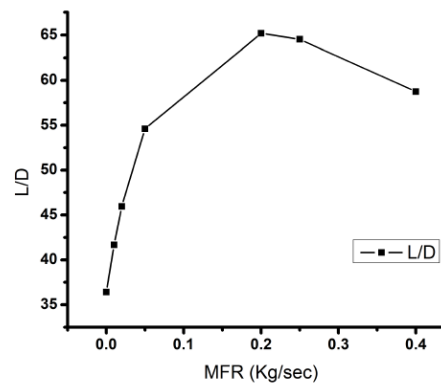


Fig. 9. L/D vs MFR for baseline NACA 0024 airfoil.

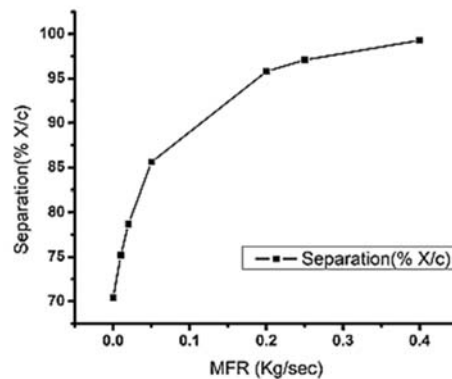


Fig. 10. Separation(% X/c) vs MFR for baseline NACA 0024 airfoil.

Figure 12 displays the pressure contour for the baseline airfoil NACA 0024 along with the velocity streamlines with an MFR of 0.20 kg/s. It is observed that the flow stays attached to the upper surface and gets separated at approximately 96% of X/c . No recirculation region is observed.

Figure 13 compares the c_p values for a baseline airfoil with and without MFR. The airfoil's upper surface

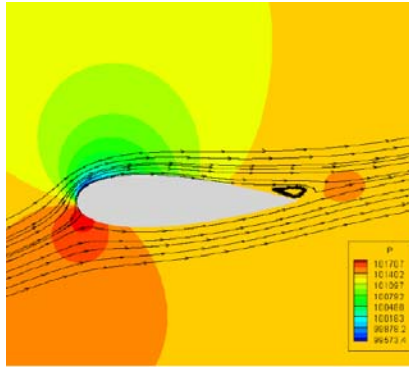


Fig. 11. Pressure contour for baseline NACA 0024 airfoil without MFR.

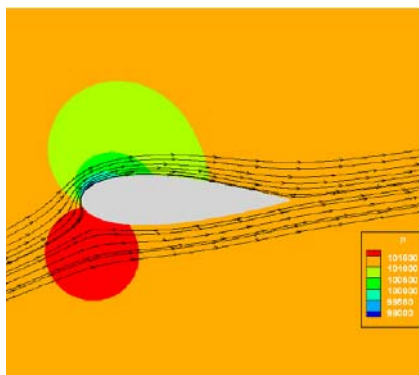


Fig. 12. Pressure contour for baseline NACA 0024 airfoil with MFR = 0.2 kg/s.

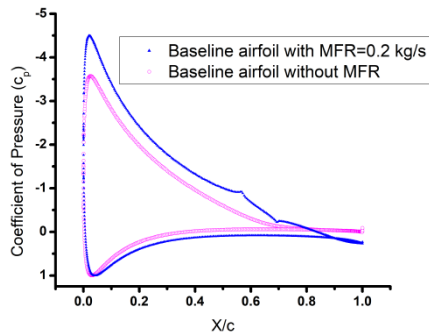


Fig. 13. Comparison of c_p along the airfoil surface for baseline airfoil with and without MFR.

has a negative c_p value, while the bottom surface has a positive value, giving lift in the upward direction. When MFR is applied to the baseline airfoil, the difference between the c_p values on the lower and upper surfaces increases, which results in increased airfoil lift. The c_p value on the upper surface steadily increases, indicating the presence of an adverse pressure gradient zone. The constant c_p indicates flow separation. It can be seen that for a baseline airfoil, the flow separates at approximately $X/c = 70\%$, as corroborated by the boundary layer's point

of $c_f = 0$ (Points of separation are specified in Table 4). However, when MFR is used, the separation point is shifted downstream of the upper surface to $X/c = 96\%$.

6.2 Parametric study on a TVC airfoil with MFR having a uniform distribution

The flow was simulated for a TVC airfoil with a variety of MFR values. A wall bleed (uniform suction) condition was applied in the segment M to N inside the cavity as indicated in Fig. 1b. Table 5 summarises the results of a TVC airfoil with various uniform MFR values.

It can be seen that when a cavity is used, attached flow on the airfoil's upper surface is obtained at a mass flow rate of 0.08 kg/s ($X_{low\ separation}^c \geq 95\%$), compared to 0.20 kg/s for the NACA 0024 baseline airfoil without a cavity.

As the MFR steadily increases, the separation point is moved further back. The trends of c_l and c_d are identical to those of a smooth airfoil. The increase in c_l value over a TVC airfoil is due to the vortex being trapped within the cavity, as demonstrated in Fig. 14. The variation in c_d in Fig. 15 indicates the important role of suction (MFR) in anchoring the vortex within the cavity. Figure 16 shows that the airfoil's L/D ratio increases with MFR and then decreases when c_d values grow. The separation point is pushed further back on the upper surface of the airfoil as the MFR increases, as illustrated in Fig. 17.

Table 5. TVC airfoil with various MFR's (uniform suction)

MFR (kg/sec)	c_l	c_d	L/D	Point of Separation (% X/c)
0.01	1.109	0.037	29.89	Recirculation zone
0.02	1.183	0.033	33.74	Recirculation zone
0.04	1.336	0.032	42.17	88.21
0.08	1.515	0.031	48.16	96.75
0.12	1.62	0.034	47.89	98.34
0.20	1.732	0.041	42.68	99.46

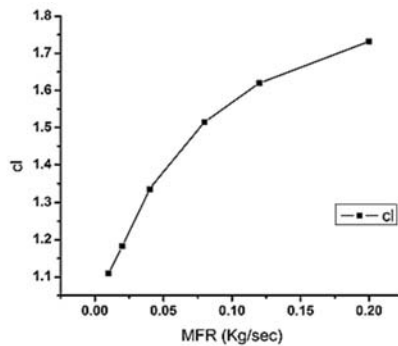


Fig. 14. c_l vs MFR on TVC airfoil (uniform suction).

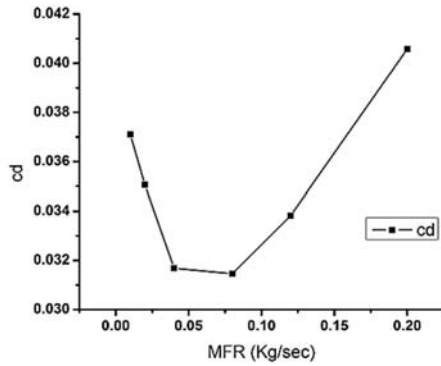


Fig. 15. c_d vs MFR on TVC airfoil (uniform suction).

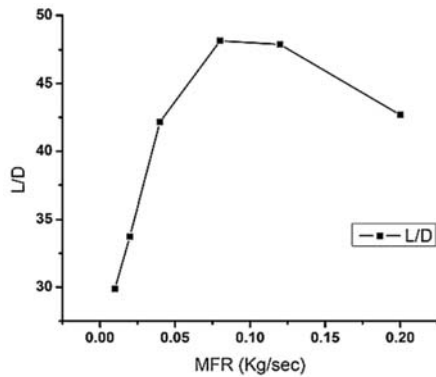


Fig. 16. L/D vs MFR on TVC airfoil (uniform suction).

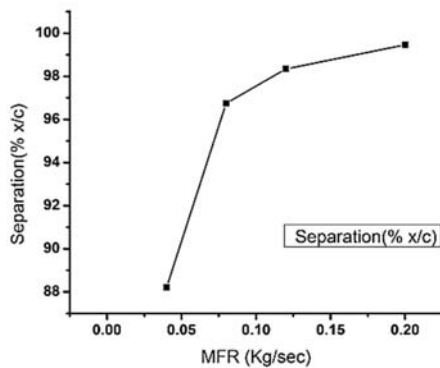


Fig. 17. Separation(% X/c) vs MFR on TVC airfoil (uniform suction).

The streamlines without MFR for a TVC airfoil are illustrated in Fig. 18. Pressure values are used to colour the streamlines. Due to the adverse pressure gradient and flow reversal, the vortex cannot be stabilised within the cavity, creating a large recirculation zone aft of the cavity. A similar observation is made for low MFR levels, as given in Table 5.

However, when the MFR is 0.10 kg/s, the separation point is pushed back, and the flow remains attached to the airfoil's upper surface, as illustrated in Fig. 19.

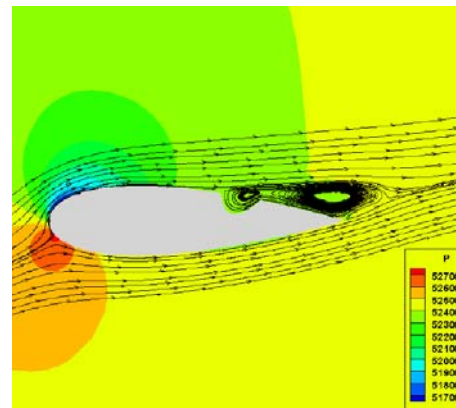


Fig. 18. Pressure contour in TVC airfoil without MFR.

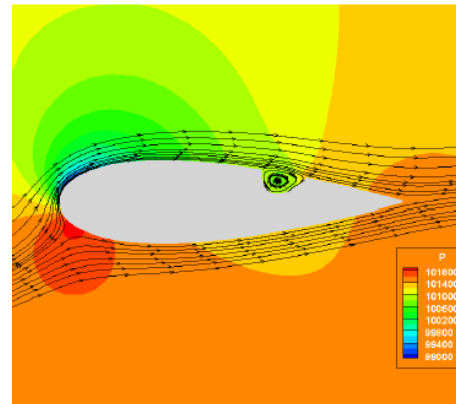


Fig. 19. Pressure contour in TVC airfoil with MFR=0.1 kg/s.

Figure 20 compares the c_p values for a TVC airfoil with and without MFR along with that of the baseline airfoil without MFR. It can be observed that, the presence of a cavity on the airfoil alone by itself, has no significant effect on the pressure distribution on the lower and the upper airfoil surface upstream of the cavity. However, when the TVC airfoil is subjected to an MFR of 0.1 kg/s, the difference between the c_p values on the lower and upper surfaces increases, resulting in an increased lift of the airfoil. It can be seen that a dip in c_p is detected at X/c corresponding to the cavity segment where suction is applied. The cavity's endpoint, i.e. X/c=0.69, denotes the cavity flow's downstream stagnation point. The reverse flow inside the cavity accelerates from the endpoint, decelerates, and then reaccelerates up to the cavity's start, i.e. X/c=0.58. This indicates the presence of a substantial recirculation zone within the cavity. The flow expands aft of the cavity segment significantly, resulting in a favourable pressure gradient and delayed flow separation.

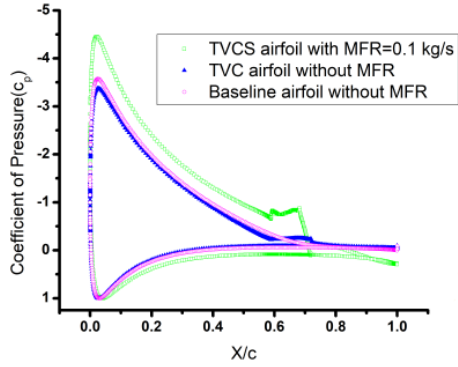


Fig. 20. Comparison of c_p along the airfoil surface for TVC airfoil with and without MFR along with baseline airfoil without MFR.

Figure 21 and Fig. 22 shows the vector plots of the velocity inside the cavity segment and at the trailing end of the TVC airfoil with and without MFR respectively.

Figure 21 illustrates mass suction applied at the base of the cavity segment. The mass suction allows the vortex to remain stabilised within the cavity, resulting in a fully attached flow aft of the cavity on the airfoil's upper surface. The stagnation region shifts slightly upstream, the flow accelerates, the boundary layer becomes thinner and more capable of withstanding an adverse pressure gradient, resulting in a downstream shift of the separation point. Without MFR, however, flow reversal indicating a trailing edge separation is shown in Fig. 22. There is no flow acceleration after the cavity's stagnation area, and the boundary layer thickens, resulting in an unfavourable pressure gradient and early flow separation.

6.3 Parametric study on TVC airfoil with MFR having a Gaussian distribution

MFR plays a vital role in anchoring the vortex in the cavity. To characterise the distribution of the MFR, a Gaussian distribution was used between the segment M to N as shown in Fig. 1b.

Gaussian function is of the form:

$$f(x) = h e^{-\frac{(x-\mu)^2}{2c^2}} \quad (1)$$

h , μ , and c are arbitrary real constants. The parameter h is the height of the curve's peak, μ is the position of the centre of the peak, and c (the standard deviation, sometimes called the Gaussian RMS width) controls the width of the "bell". Gaussian curves for various μ values and with different areas are shown in Fig. 23.

Cumulative MFR was distributed as a Gaussian curve, and the area under the curve gives the net MFR value. The distribution was parameterized with three variables.

MFR = cumulative suction value

h = height of the peak

μ = mean value of the Gaussian distribution indicating the position of the peak.

The Gaussian function's c parameter is set to 1/6 of the segment A to B length to account for the Gaussian curve's spread. These three parameters are interdependent by this equation

$$\int_a^b h \exp\left(-\frac{(x-\mu)^2}{2c^2}\right) dx = \sqrt{\frac{\pi}{2}} ch \left(\operatorname{erf}\left(\frac{\mu-a}{\sqrt{2}c}\right) - \operatorname{erf}\left(\frac{\mu-b}{\sqrt{2}c}\right) \right) \quad (2)$$

where, erf is the error function.

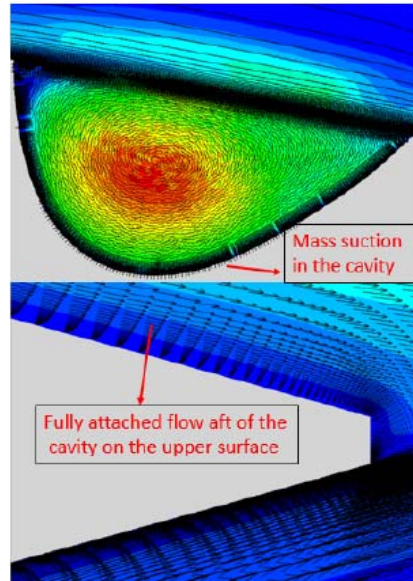


Fig. 21. Vector plot of velocity streamlines inside the cavity for TVC airfoil with MFR=0.1 kg/s.

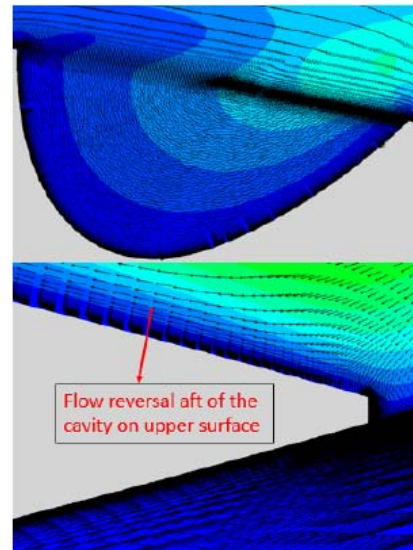


Fig. 22. Vector plot of velocity streamlines inside the cavity for TVC airfoil without MFR.

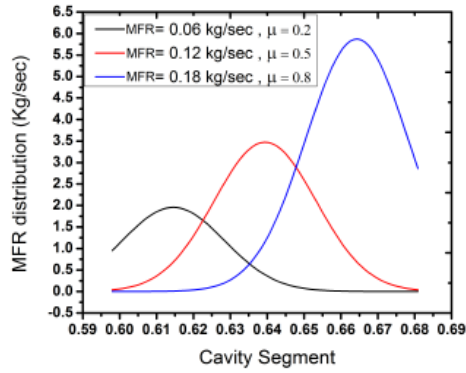


Fig. 23. Gaussian curves for various μ values and with different area.

Numerical bounds for the parameters

The following bounds were decided for the above mentioned parameters.

1. Because ' μ ' represents the Gaussian curve's mean value, it can range from $\mu = 0$ to $\mu = 1$. μ denotes the location of the Gaussian distribution's peak. The change in μ from 0 to 1 reflects a change in the peak suction from $X/c = 0.58$ to $X/c = 0.69$, or from point A to point B in Fig. 1b.

2. Given that MFR is a measure of additional energy input, the objective is to capture the vortex with the lowest MFR possible. Because MFR is a physical quantity, it cannot be negative. According to a parametric study on the smooth airfoil, the MFR should be less than 0.2 kg/sec to reap the cavity's benefits.

3. The value of h is calculated from the abovementioned equation, and hence no numerical bounds are specified.

Figure 24 illustrates the relationship between L/D and μ for various MFRs. Figure 25 illustrates the relationship between the separation point (% X/c) and μ for various MFR's. Higher L/D is achieved for a particular MFR value for $\mu = 0$ and $\mu = 1$, i.e. when the mass suction is concentrated on either ends of the cavity segment. It may be concluded that when suction is concentrated on either ends of the cavity segment at a certain MFR value, the separation point is pushed back on the airfoil's upper surface. Thus, extreme values of μ are advantageous for increasing the L/D ratio and delaying separation.

Figure 26 and Fig. 27 depict the c_l and c_d curves for various MFR values at the suction peak's two extreme locations, $\mu = 0$ and $\mu = 1$ respectively. When compared to the cases with a uniform suction distribution (Section 6.2), the c_d values are high. However, because c_l is also a large value, the overall L/D ratio is improved. Additionally, when the suction peak is positioned in the front half of segment M to N ($\mu = 0$), the drag decreases initially before increasing as the MFR increases. This is because a suction component operates in the direction of

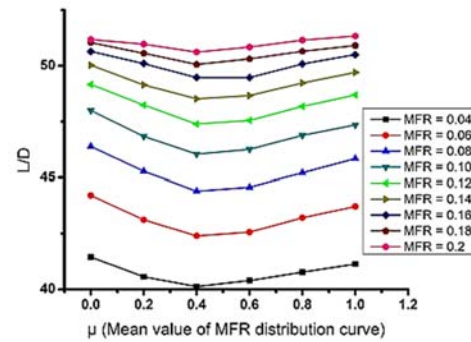


Fig. 24. L/D vs μ for various MFR's.

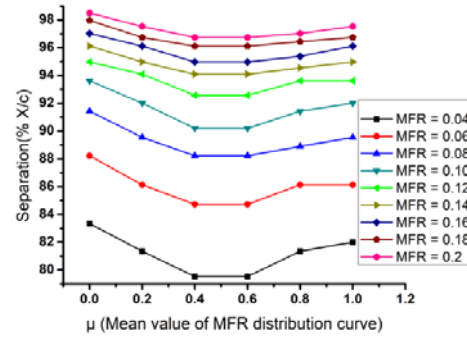


Fig. 25. Separation vs μ for various MFR's.

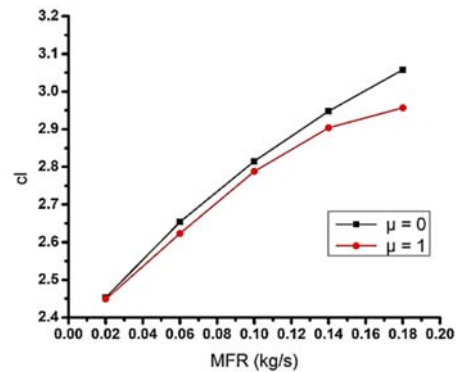


Fig. 26. c_l vs MFR for $\mu = 0.1$ for various MFR's.

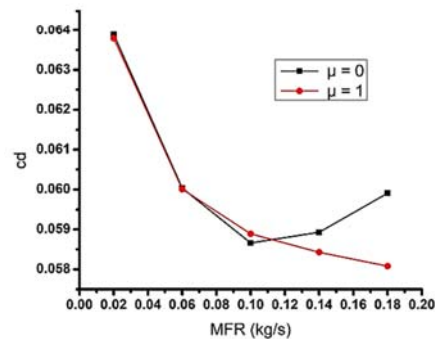


Fig. 27. c_d vs MFR for $\mu = 0,1$ for various MFR's.

velocity, increasing drag. In comparison, when the suction peak is located at the rear end of the M to N segment ($\mu = 1$), the drag reduces as the MFR increases. In this instance, a suction component acts in the opposite direction as drag.

6.4 Inferences from the parametric study and the need for optimisation

The following points can be inferred from the parametric study:

1. Trapping a vortex is possible inside a cavity. However an active mass suction (MFR) is required to stabilise the vortex and move the flow separation to the aft end of the cavity.
2. L/D increases with an increase in MFR for a NACA 0024 baseline airfoil, and flow remains attached at very high MFR. However, in the presence of a cavity, a lower value of MFR is sufficient to anchor the vortex inside the cavity and delay the flow separation.
3. It was discovered that a point suction, denoted as MFR applied on each end of the cavity section, outperforms the Gaussian distribution of MFR. However, providing a point suction to the cavity segment is not viable. Suction velocity must be increased to maintain the same MFR, as the suction area is significantly smaller than the distributed suction area. Distributed suction appears to be a more viable solution.

These inferences led to an optimisation analysis of the cavity shape and MFR to maximize the L/D and attached flow on the airfoil's upper surface.

7. VARIATION OF TVC SHAPE

A 3rd-order Bezier curve was used for cavity parameterisation. As the curve is completely contained in the convex hull of its control points, it can be graphically displayed and used to manipulate the curve intuitively, as shown by Donelli *et al.* (2011).

A 3rd-order Bezier curve is of the following form as shown by Piegl and Tiller (1996):

$$f(t) = (1-t)^3 + 3(1-t)^2 \cdot t + 3(1-t) \cdot t^2 + t^3 \quad (3)$$

Following parameters are required to define a

Bezier curve as can be seen from Fig. 28.

1. Slope at point A ($m1$)
2. Slope at point B ($m2$)
3. Location of point C
4. Slope at point C ($m3$)

8. OPTIMIZATION METHODOLOGY

The operation was automated using Esteco modeFRONTIER software. The optimisation methodology employed was the built-in Multi-Objective Genetic Algorithm (MOGA-II). The design space was initiated with ten designs using

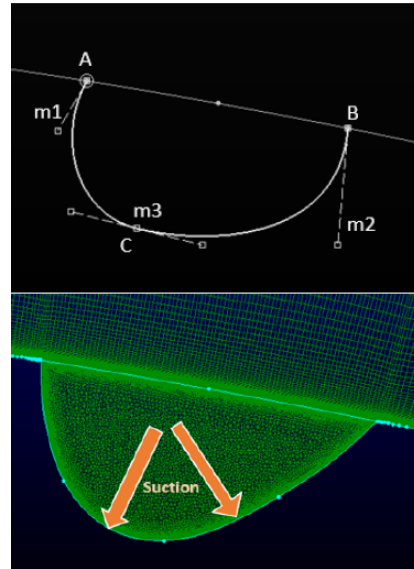


Fig. 28. Parameters used to define the cavity and suction segment.

Table 6. Multi-objective optimization

Objective	Constraints
Maximize L/D	Fully attached flow $\frac{X_{\text{flow separation}}}{c} \geq 95\%$
Minimum Suction	Width of the cavity (Distance between point A and B) Depth of the cavity $\leq 40\% \text{ of } \frac{t_{\text{max}}}{c}$

Uniform Latin Hypercube (ULH) sampling. The optimisation process was iterated over 25 generations. The purpose of this study is to improve the geometry of a fixed-depth, fixed-width cavity in order to maximize aerodynamic efficiency (L/D) and reduce the mass suction required to stabilize the vortex inside the cavity. The constraint of delayed separation was imposed on the airfoil's upper surface under the initial conditions specified in Table 1 as illustrated in Table 6. The flowchart of the optimisation process is depicted in Fig. 29.

9. RESULTS

Using an initial design space of 10 designs, 250 design points were obtained after 25 generations. Figure 30 illustrates the Pareto optimal front achieved after 25 generations of optimisation using a genetic method. Here, L/D is displayed versus suction mass flow rate, and the coloured bubbles indicate the chord length at which the point of separation occurs. Each bubble corresponds to a unique cavity form. Figure 31 is a 4D bubble plot showing the variation of c_1 and c_d for different cavity

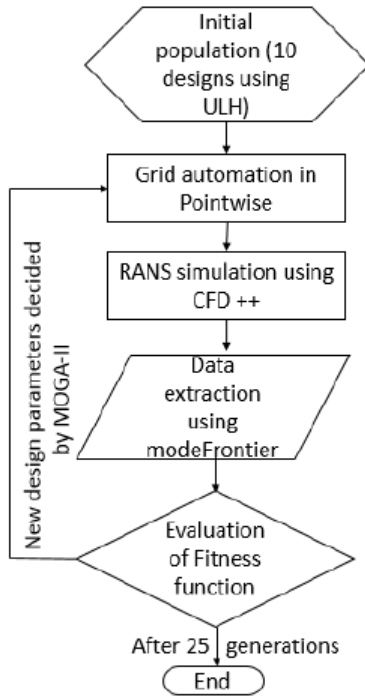


Fig. 29. Flow chart for optimization.

shapes at various MFR's. The colored bubble shows the suction MFR value and the diameter of the bubble represents the value of L/D for a given cavity shape. As illustrated in Fig. 30, the best L/D values are obtained at around MFR=0.1 kg/s. This relates to low c_d values, as illustrated in Fig. 31. Any additional increase in c_i by increasing MFR results in a drag penalty, which reduces the L/D.

It can be observed that the design space is completely distributed, and optimum designs can be produced by making a trade-off between two objectives, namely L/D and MFR while keeping the delayed separation limitation in mind. Because MFR represents the additional energy input to the cavity, a low value is desired. However, as the MFR value decreases, the L/D decreases as well, and the flow separates early, at around 60% X/c on the airfoil's upper surface. Additionally, it demonstrates that the optimal designs are centred on MFR values between 0.08 and 0.16 kg/s, satisfying the restriction of fully attached flow. The optimal shapes corresponding to the 25th generation have been recovered, and a selection of the optimised design shapes and their associated properties are listed in Table 7. The Design ID: 71 is the optimal design in terms of the highest L/D ratio and delayed separation point (% X/c) with the least amount of mass suction required to stabilise the vortex inside the cavity.

Figure 32 shows the pressure contour along with the velocity streamlines for the airfoil with design ID:71 along with the velocity streamlines. It can be observed that the vortex is stabilised inside the cavity

and the flow remains attached on the upper surface of the airfoil resulting in a higher value of L/D.

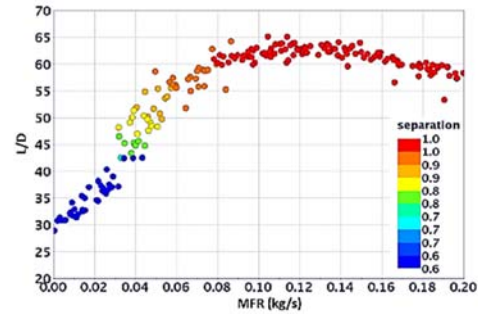


Fig. 30. L/D vs MFR plot where colour represents the point of separation in terms of the chord length.

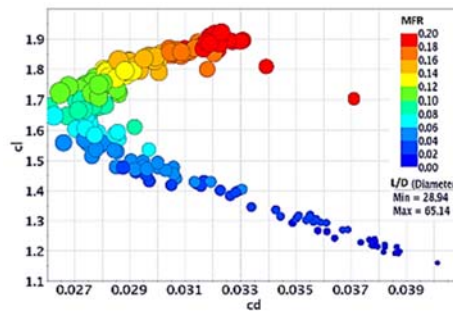


Fig. 31. c_i vs c_d plot where colour represents MFR and diameter of bubbles represent L/D.

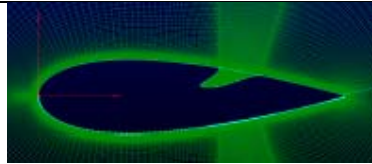
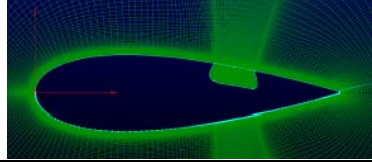
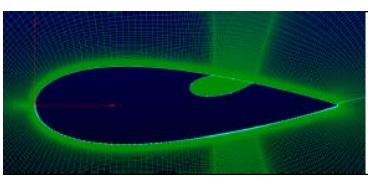
To arrive at an objective conclusion, the design ID:71 with a MFR of 0.1 kg/s was chosen, and an off-design analysis was performed at several different incidence angles, with the results compared to the NACA 0024 baseline airfoil.

Figure 33 illustrates the fluctuation in L/D with AoA, which ranges from 2° to 16° . It is noted that the optimised TVCS airfoil with Design ID:71 has a greater L/D for all incidences and a higher stall angle of AoA= 14° compared to AoA= 10° for the baseline airfoil.

10. CONCLUSION

The role of a trapped vortex cavity in preventing separation and optimising an airfoil's aerodynamic performance is investigated. Numerous parametric studies have been conducted to examine the role of each parameter critically. In cases without suction, early separation of the flow can be observed. A minimum suction rate of 0.2 kg/sec is required for the baseline airfoil for a fully attached flow (separation at 95% of X/c) whereas, the same could be achieved at a lower suction rate of 0.08 kg/s for a TVC airfoil. The parametric study concluded that both mass suction and cavity shape play a crucial role in anchoring the vortex inside the cavity. A multi

Table 7. Some designs obtained from optimisation along with their specifications

Design Id	Shape	MFR (kg/s)	c_l	c_d	L/D	Point of Separation (% X/c)
16		0.087	1.667	0.027	61.55	95.76
71		0.106	1.737	0.028	62.92	97.77
208		0.105	1.722	0.028	62.40	97.03

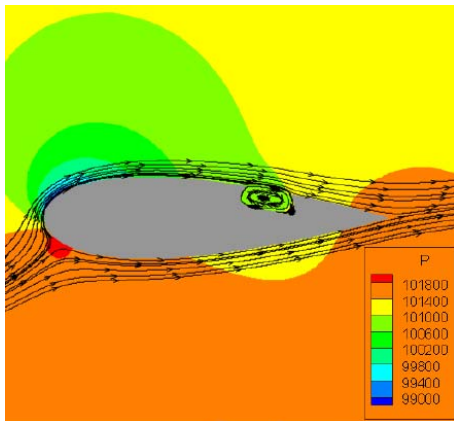


Fig. 32. Pressure contour for Design ID:71 (TVCS).

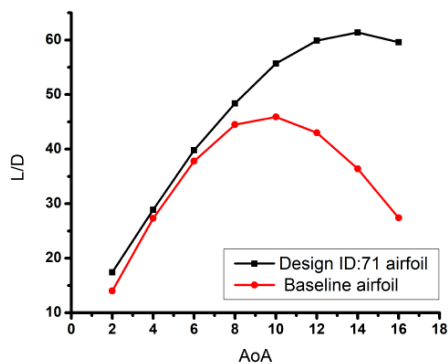


Fig. 33. L/D vs AoA for Design Id: 71 (TVCS) comparing with the baseline airfoil.

-objective optimisation study was carried out using the genetic algorithm to design the cavity shape in the baseline NACA 0024 airfoil to enhance aerodynamic characteristics. The cavity shape and suction mass flow rate have been optimised to maximize L/D. It is demonstrated that by optimising the cavity shape, the mass suction required to anchor the vortex inside the cavity and maintain the flow to be attached to the upper surface can be minimized. A set of optimum designs were obtained from the study. In order to reach an objective conclusion, an off-design analysis was performed on one of the optimised designs and compared to the baseline airfoil at various incidences. It was observed that the optimised design has a higher L/D ratio than the baseline airfoil for the entire range of incidences.

ACKNOWLEDGMENTS

The authors acknowledge the support provided by the Department of Aerospace Engineering, IIST, Thiruvananthapuram, India in carrying out this research work.

REFERENCES

- Adkins, R. (1975). A short diffuser with low pressure loss. *Journal of Fluids Engineering*, 297–302.
- De Gregorio F, F. G. (2008). Flow control on a high thickness airfoil by a trapped vortex cavity. *14th International Symposium on Applications of Laser Techniques to Fluid Mechanics*.
- Donelli, R., F. De Gregorio and P. Iannelli (2010). Flow separation control by trapped vortex. In *48th AIAA Aerospace Sciences Meeting*

- Including the New Horizons Forum and Aerospace Exposition*, 1409.
- Donelli, R., P. Iannelli, S. Chernyshenko, A. Iollo and L. Zannetti (2009). Flow models for a vortex cell. *AIAA journal* 47(2), 451–467.
- Donelli, R. S., P. Iannelli, E. Iuliano and D. De Rosa (2011). Suction optimization on thick airfoil to trap vortices. *Physics and Fluids Unit, Centro Italiano Ricerche Aerospaziali (CIRA), Via Maiorise, snc, Italy 81043*.
- Iollo, A. and L. Zannetti (2001). Trapped vortex optimal control by suction and blowing at the wall. *European Journal of Mechanics B/Fluids* 20(1), 7–24.
- Kasper, W. A. (1975). Some ideas of vortex lift. Technical report, SAE Technical Paper.
- Lasagna, D., R. Donelli, F. De Gregorio and G. Iuso (2011). Effects of a trapped vortex cell on a thick wing airfoil. *Experiments in fluids* 51(5), 1369–1384.
- Olsman, W. and T. Colonius (2011). Numerical simulation of flow over an airfoil with a cavity. *AIAA journal* 49(1), 143–149.
- Piegl, L. and W. Tiller (1996). *The NURBS book*. Springer Science & Business Media.
- Ringleb, F. O. (1961). Separation control by trapped vortices. *Boundary layer and flow control 1*, 265.
- Rockwell, D. and E. Naudascher (1979). Self-sustained oscillations of impinging free shear layers. *Annual Review of Fluid Mechanics* 11, 67–94.
- Rossiter, J. (1964). Wind-tunnel experiments on the flow over rectangular cavities at subsonic and transonic speeds. *Aero Res Counc (No. 3438)*.
- Rowley, C., T. Colonius and A. Basu (2001). On self-sustained oscillations in two dimensional compressible flow over rectangular cavities. *Journal of Fluid Mechanics*, 315–345.
- Rowley, C., V. Juttijudata and D. Williams (2005). Cavity flow control simulations and experiments. In *43rd AIAA Aerospace Sciences Meeting and Exhibit*, 292.
- Vuddagiri, A. and A. Samad (2013). Vortex trapping by different cavities on an airfoil. *Wind Engineering* 37(5), 469–482.